JOURNAL OF APPLIED ELECTROCHEMISTRY 25 (1995) 425–432

The manganese dioxide electrode Part XII: Gibbs free energy of H insertion compounds and a planar model

F. L. TYE, S. W. TYE*

Energy Technology Centre, Middlesex University, Bounds Green Road, London N11 2NQ, Great Britain

Received 14 July 1994; revised 11 October 1994

Experimental values for the Gibbs 'free energy of mixing' of solid solutions produced by electrochemical H insertion into a commercial synthetic γ-MnO_2 have been derived from published electrode potential measurements carried out in Leclanché electrolyte. Calculated values are based on the reasonable assumption that the solid solutions are thermodynamically ideal so that the Gibbs free energy of mixing can be estimated from the positional entropy of the inserted species. Comparison of the two sets of values provides strong evidence that the inserted H is present as two thermodynamically independent species H^+ and e at least up to 40% fill. Additional insight is provided by a planar random insertion model. The model shows the development of microdomains of fully H inserted material at the higher levels of insertion but prior to complete insertion as is required to explain published experimental phenomena. The model also allows the calculation of the Gibbs free energy of mixing to be refined to take into account either the stabilisation of certain H^+e pair types or restriction in the movement of the H^+ and e species of pairs caused by adjacent pairs blocking pathways. The latter refinement gives very good agreement with the experimental data using one adjustable parameter namely a blocking efficiency of 50%.

1. Introduction

H insertion into manganese dioxide prepared commercially by electrodeposition and from other sources is important technologically and scientifically. Technologically, it is the primary cathodic process which occurs when Leclanché and alkaline manganese batteries are discharged [1]. The thermodynamics of the process, the diffusion rate of the inserted species and the stability of the ensuing insertion compounds in the battery electrolyte determine battery performance [1–3]. Scientifically the process is of interest because measurement of electrode potential gives access to the Gibbs free energies of the insertion compounds, which form a continuous solid solution, via the relationship

$$G_s = G_0 - F\int_{s=0}^{s}\left(E_s + \frac{2.303\,RT}{F} \times \mathrm{pH}\right)\mathrm{d}s \qquad (1)$$

where G_s and G_0 are the Gibbs free energies in joules per mol at insertion levels of s and zero moles of inserted H per mole of manganese dioxide, respectively; E_s is the electrode potential in volts with respect to the standard hydrogen electrode at an insertion level of s and R, T and F have their usual significance. Surprisingly this route to the Gibbs free energies of the H insertion compounds of manganese dioxide does not appear to have attracted much attention.

The ratio of oxygen to manganese obtained by the usual analytical procedures [4] is always less than two for manganese dioxides which are battery active. It has become the convention to assume that this is due to the initial presence of some inserted H so that all insertion compounds can be represented by the general formula $MnOOH_r$ with r having a value of about 0.1 initially and 1 when insertion is complete [5–7]. A careful analysis of this approach, however, showed that the mandatory Gibbs–Duhem relation for the solid solutions was only obeyed if a major proportion of the inserted H, initially assumed to be present in the starting manganese dioxide, was electrochemically inactive [8]. For various models which match quite closely the change of electrode potential with H insertion, 0.08 [9–11] or 0.0865 [12] moles of inserted H per mole of manganese dioxide was assumed to be electrochemically inactive for a material with an initial composition represented as $MnOOH_{0.105}$. Thus approximately 80% of the H inserted to explain the stoichiometry was regarded as electrochemically invisible. Rather than persist with this contrived situation it seems preferable to assume that the starting material is actually oxygen deficient with a stoichiometry of MnO_n where $n < 2$. Electrochemical discharge may then be represented as

$$MnO_n + sH^+ + se \longrightarrow MnO_nH_s \qquad (2)$$

* Present address: Sandoz Institute for Medical Research, 5 Gower Place, London WC1E 6BN.

0021-891X © 1995 Chapman & Hall

The proposition of oxygen deficiency does not conflict with Ruetschi's cation vacancy theory [13] but does require the oxygen deficiency to be greater than the cation vacancies. The loss of positive charge arising from a Mn^{4+} vacancy is compensated in Ruetschi's proposal by four H^+ species on adjacent O^{2-} sites which are held in position by the need to compensate for the charge loss at the cation vacancy site. While this postulate provides a likely explanation of the source of that part of the water only driven off at temperatures significantly above 100 °C, it does not explain the oxygen deficient stoichiometry revealed by analysis. Furthermore, because their location is fixed, these charge compensating H^+ species do not contribute to positional entropy, which is the key concept considered in the next Section.

2. Gibbs free energy of mixing

Application of Equation 1 requires careful choice of discharge conditions if the derived thermodynamic quantities are to have significance.

While discharge in concentrated KOH solution is superficially attractive as pH changes arising from discharge are minimal, there is a serious complication which is often overlooked. At high insertion levels the solid solutions are unstable in concentrated KOH solutions [3] and in consequence the electrode potentials measured are not representative of the H insertion compounds.

In the alternative medium of Leclanché electrolyte only the first stage of discharge, while solid NH_4Cl is present in the cathode mixture, takes place in an invariant electrolyte [1, 2]. This difficulty has been overcome by the use of excess solid NH_4Cl so that some was still present in the cathode mix at the completion of discharge [9]. Data obtained in this way has been tabulated [7]. In addition to minimal corrections for electrolyte effects, the discharge used was very slow, taking more than 50 days to complete, with 12 h recuperation allowed before recording the daily potential so that overpotential errors were also minimised. In this careful work [9] the composition of the solid solution was corrected for the dissolution of Mn^{2+} which occurred in the later stages of discharge. This correction was minimized by limiting the amount of electrolyte present [14]. With some manganese dioxides hetaerolite is an alternative product of discharge to the H insertion compounds [2, 15–18]. X-ray diffraction did not reveal the presence of hetaerolite [14] in the work outlined above.

For the reasons just described the data of Maskell *et al.* [7, 9] have been selected as the basis for the application of Equation 1. These voltage data are plotted against insertion levels s in Fig. 1. The figure shows that a maximum insertion level of 0.875 moles of H per mole MnO_n was achieved and that the electrode potential decreased in the S-shape expected of a solid solution.

Formally any composition of solid solution, MnO_nH_s, can be considered as arising from a mixture of the end-compounds MnO_n and $MnO_nH_{s(max)}$ where s(max) is 0.875 per mole MnO_n for the manganese dioxide under consideration. Thus 1 mole of MnO_nH_s comprises $(s/0.875)$ moles of $MnO_nH_{0.875}$ and $(1 - s/0.875)$ moles of MnO_n and the Gibbs free energy for the insertion compound of this composition, G_s, is given by

$$G_s = (s/0.875)G_{0.875} + (1 - s/0.875)G_0 + \Delta G_{mix} \quad (3)$$

where $G_{0.875}$ and G_0 are the Gibbs free energies of 1 mole of $MnO_nH_{0.875}$ and MnO_n, respectively, and ΔG_{mix} is the Gibbs free energy of mixing. Rearranging and introducing Equation 1:

$$\Delta G_{mix} = F\left[\frac{s}{0.875}\int_{s=0}^{s=0.875}\left(E_s + \frac{2.303\,RT}{F} \times \mathrm{pH}\right)\mathrm{d}s - \int_{s=0}^{s}\left(E_s + \frac{2.303\,RT}{F} \times \mathrm{pH}\right)\mathrm{d}s\right] \quad (4)$$

Thus ΔG_{mix} can be experimentally determined from the data presented in Fig. 1.

Experimental estimation of the Gibbs free energy of mixing is important for comparison with theoretical models in order to establish whether the inserted H is present as thermodynamically independent entities H^+ and e [19] or as associated pairs H^+e. The theoretical models assume that the solid solution is ideal so that the Gibbs 'free energy of mixing' can be directly related to the 'entropy of mixing', ΔS_{mix} [7, 10, 20]

$$\Delta G_{mix} = -T\Delta S_{mix} \quad (5)$$

Thermodynamically ideal solutions arise from mixing compounds with very similar constitutional

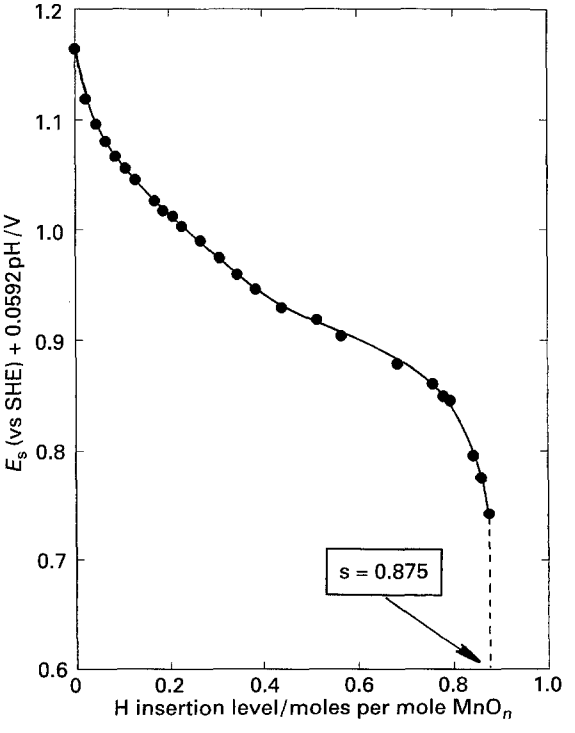

Fig. 1. Electrode potential against H insertion level.

characteristics [20]. It is entirely reasonable that the H insertion compounds should be so regarded as the ionic frameworks of the end-compounds, MnO_n and $MnO_nH_{s(max)}$, are similarly organised and the only difference is the presence of inserted H in one of them [9, 14, 21].

The additional positional entropy which occurs on mixing $MnO_nH_{s(max)}$ with the starting material MnO_n is due to the additional sites available for the inserted H and may be estimated using the relationship [7, 10, 22, 23]

$$\Delta S_{mix} = k \ln W_s \quad (6)$$

where k is Boltzmann's constant and W_s is the number of ways that s moles of inserted H can be arranged in 1 mole of MnO_nH_s. On the basis that s(max) defines the number of sites available, the number of ways, w_s, that s moles of a single component can be arranged on the sites of 1 mole MnO_nH_s is given by the relationship

$$w_s = \frac{[N_A s(\max)]!}{[N_A s]![N_A\{s(\max) - s\}]!} \quad (7)$$

where N_A is Avogadro's number. Two possibilities can be identified. If the inserted H is present as a single thermodynamic component due to the association of inserted H^+ and e species albeit on different parts of a single site with H^+ located on oxygen ions and e on a manganese ion, then ΔG_{mix} is obtained from Equations 5 and 6 by equating W_s with w_s obtained from Equation 7. However, if H^+ and e are thermodynamically independent then the number of ways that the two components can be arranged is w_s^2. These alternatives can be accommodated by rewriting Equations 5 and 6 as

$$\Delta G_{mix} = -\phi kT \ln w_s \quad (8)$$

where ϕ is 1 or 2 according to whether the inserted H^+ and e species are associated or independent, respectively. By using Stirling's approximation for large numbers,

$$\ln Y! = Y \ln Y - Y \quad (9)$$

the value of 0.875 for s(max), Equations 7 and 8 can be combined into a form for direct comparison with the experimentally derived Gibbs free energy of mixing

$$\Delta G_{mix} = -\phi RT[0.875 \ln 0.875 - s \ln s - (0.875 - s) \ln (0.875 - s)] \quad (10)$$

The comparison of Equation 10 with the experimental data is shown in Fig. 2. The important conclusion is that the inserted H^+ and e species are thermodynamically independent. For insertion levels up to $s = 0.35$ (40% fill) the match of the experimental data with Equation 10 using $\phi = 2$ is very good. For $s > 0.35$ the experimental data falls slightly above the theoretical curve suggesting some association of H^+ and e species. The complete absence of adjustable parameters from Equation 10 makes this evidence of the independence of inserted H^+ and e within the manganese dioxide framework particularly convincing.

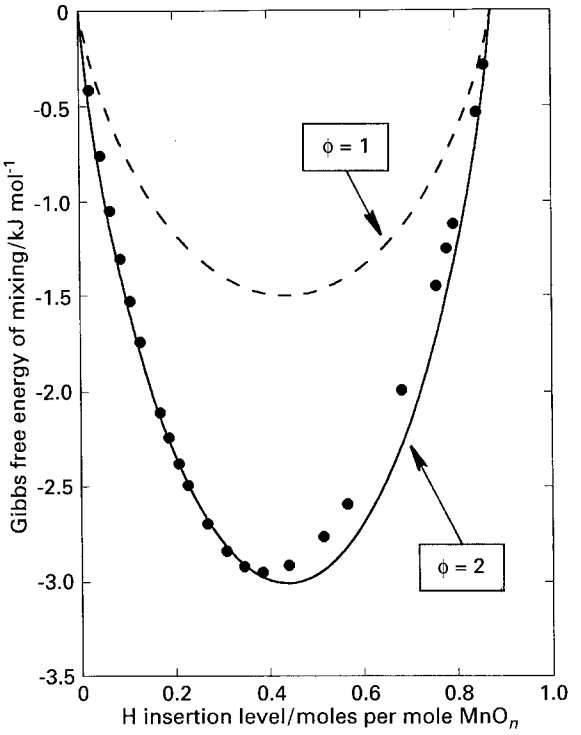

Fig. 2. Gibbs free energy of mixing against H insertion level. Key: (•) experimental data derived with Equation 4; (– – –) Equation 10 with $\phi = 1$; and (——) Equation 10 with $\phi = 2$.

3. Planar model

The basis of Equation 6 is that all possible arrangements for inserted H^+ and e are equally probable. This requirement plus the deduction that the inserted H^+ and e species are thermodynamically independent opens the way to the development of a random insertion model in order to gain further insight.

Electrodeposited manganese dioxide (EMD) is perhaps best represented as an intergrowth of ramsdellite and pyrolusite [24–27]. The crystal structure of both minerals may be represented as layers of hexagonally packed oxygens in the *bc* plane with the planes combined to give a hexagonally close-packed structure of oxygens. Only the arrangements of the manganese ions in half of the spaces which are octahedrally coordinated with oxygens distinguish ramsdellite [28] and pyrolusite [29]; or indeed ϵ-MnO_2 [30], a possible alternative crystalline structure for EMD [7, 31], or microtwinned variants invoked to explain the paucity of X-ray diffraction lines [32, 33]. The model chosen is a slab in the *bc* plane of one unit cell thickness. The full structure consists of identical slabs added above and below the chosen slab. Figures 3 and 4 show that the slabs for pyrolusite and ramsdellite lead to hexagonal projections of the oxygen network on the *bc* plane with manganese ions sited within the hexagons at depths in the slab of 0.25 or 0.75 of the thickness. The depths of manganese ions in the slab are disregarded in the

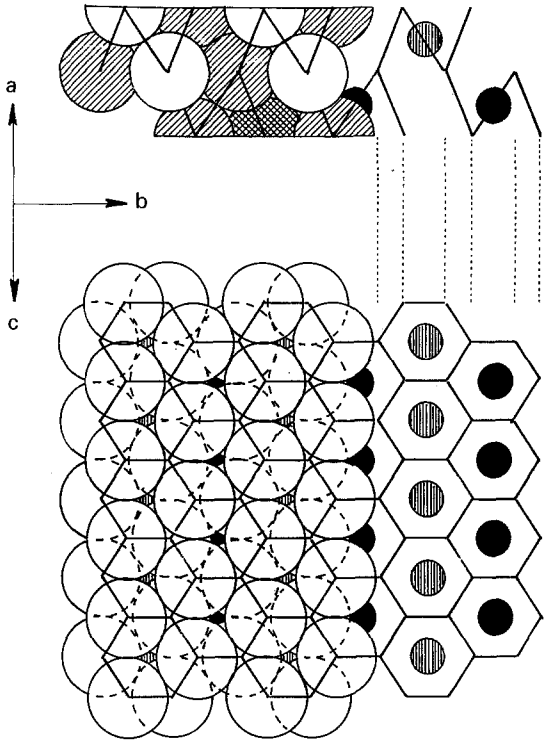

Fig. 3. Planar model of pyrolusite.

model and in consequence ramsdellite, pyrolusite, their intergrowths and microtwinned variants, and ϵ-MnO_2 can all be represented by a network of hexagons joining the oxygen sites with manganese sites at the centres of each hexagon. The model is thus independent of the precise crystalline structure allocated to EMD.

Figure 5 shows the 2500 site array used for simulated insertions. The array is wrapped so that sites 1 to 50 are adjacent to sites 2451 and 2500 and sites 1/51 to 2401/2451 are adjacent to sites 50/100 to 2450/2500. This eliminates edge effects. Sites for insertion

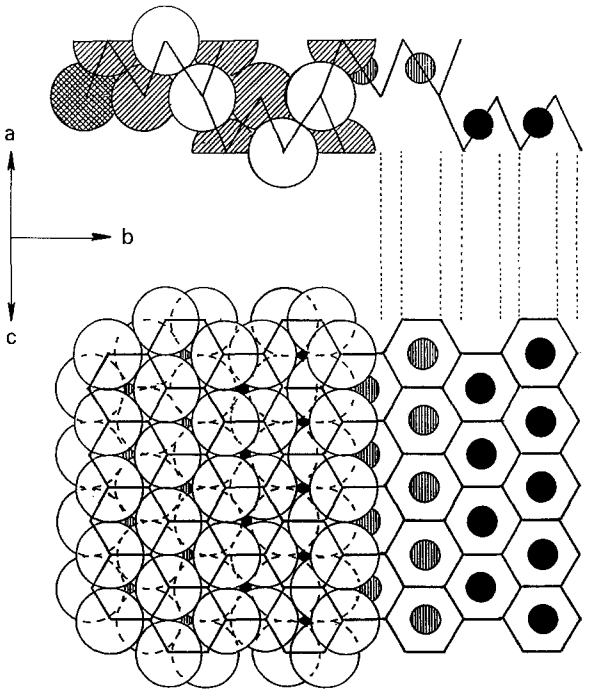

Fig. 4. Planar model of ramsdellite.

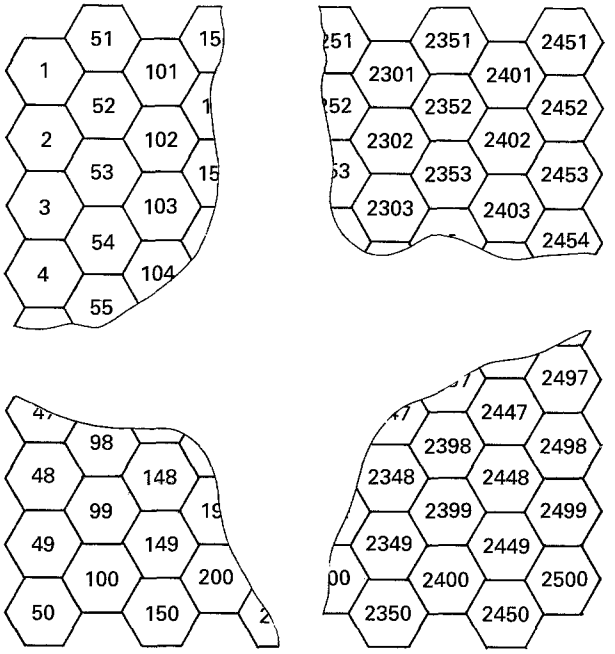

Fig. 5. Array of 2500 sites.

of H^+ and e were alternatively chosen at random using a random number generator 'ran2' [34] until all the sites were occupied. The symbolism used for site occupancy is shown on an enlarged scale in Fig. 6. As insertion was random each run produced a different pattern of insertion. One thousand runs were therefore carried out and Fig. 7 depicts the progression of insertion for the 'average' run. The method of selecting the 'average' run will be described shortly.

Perhaps the most significant features which are apparent at low insertion levels are (a) that only a small fraction of the inserted H^+ and e species occupy identical sites, i.e., are present as pairs, and (b) that small clusters of unpaired H^+ and unpaired e species are formed. While these features are consequences of the model they are primarily outcomes arising from the experimental values of the Gibbs free energy of mixing. The clusters of species carrying identical charge require further comment as such arragements might be considered unlikely because of charge repulsion. That this is not so is due to the charged framework of the host lattice. Thus the repulsion between adjacent Mn^{4+} ions would be reduced not increased by insertion of electrons since the charge

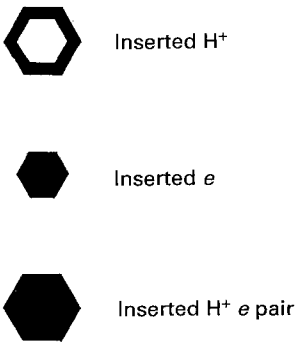

Fig. 6. Symbolism used for site occupancy.

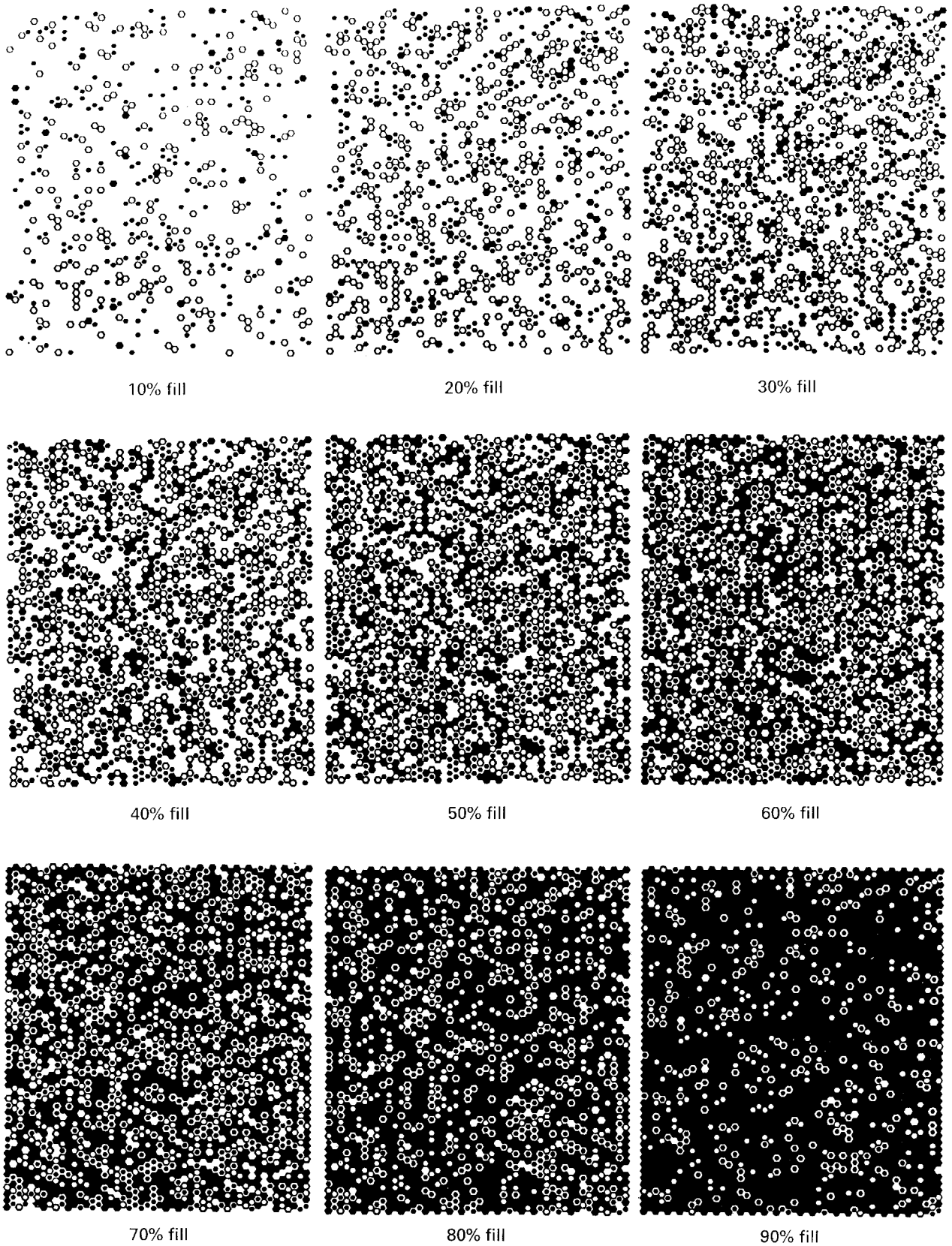

Fig. 7. Progression of H^+e insertion for the 'average' run.

on each manganese would be reduced from +4 to +3. Similarly the insertion of H^+ onto adjacent O^{2-} sites would reduce charge repulsion. A further factor which may stabilize independent arrangements of inserted H^+ and *e* species is an appropriate adjustment of the 3*d* electron cloud in a manner which acts similarly to the solvation of ions in aqueous solution.

At intermediate levels of insertion, an increasing proportion of the inserted H^+ and *e* species are paired on sites and small clusters of pairs on adjacent sites begin to form. The structure of the model is such that each pair can have up to six pairs as adjacent neighbours. For the 'average' run pairs with all six adjacent sites also occupied by pairs commence forming just below 60% fill. The process continues so that at high levels of insertion, microdomains of the end-product appear to exist. This is evident from inspection of the situation at 80% and 90% fill depicted in Fig. 7. The possibility, therefore, arises that at high levels of insertion, microdomains of the end-product become stabilised or crystallise in the structure and are thereby removed from contributing to the Gibbs free energy of mixing. Evidence for microdomains may be adduced from a recent X-ray investigation [21]. In this work new X-ray diffraction lines characteristic of the final product first appeared at about 80% fill. The other X-ray diffraction lines which originated from the solid solution continued to shift with insertion level indicating coexistence of solid solution and final product at the higher levels of insertion. In this region H mobility also appeared to be partially restricted which would be consistent with the presence of stable microdomains of the end-product.

The progress of simulated insertion was followed for each of the 1000 runs by counting the numbers of the following:

unpaired H^+ or *e* species
isolated pairs (type O)
pairs with 1 other pair as a near neighbour (type I)
pairs with 2 other pairs as near neighbours (type II)
pairs with 3 other pairs as near neighbours (type III)
pairs with 4 other pairs as near neighbours (type IV)
pairs with 5 other pairs as near neighbours (type V)
pairs with all 6 near neighbours as pairs (type VI).

These numbers are mutually exclusive, that is, their sum is the total number of either H^+ or *e* species inserted. The values of the above counts averaged over the 1000 runs and expressed as a fraction of the total number of H^+ or *e* species inserted are plotted against percentage fill in Fig. 8.

The 'average' run used for displaying the progress of insertion was selected in the following way. At each 2% of fill, the forty runs which gave counts for each pair type O to VI closest to the average values were identified. The run which was identified the most number of times was designated the 'average' run.

Figure 8 shows that although more than one type of pair are normally present at each percentage fill, each

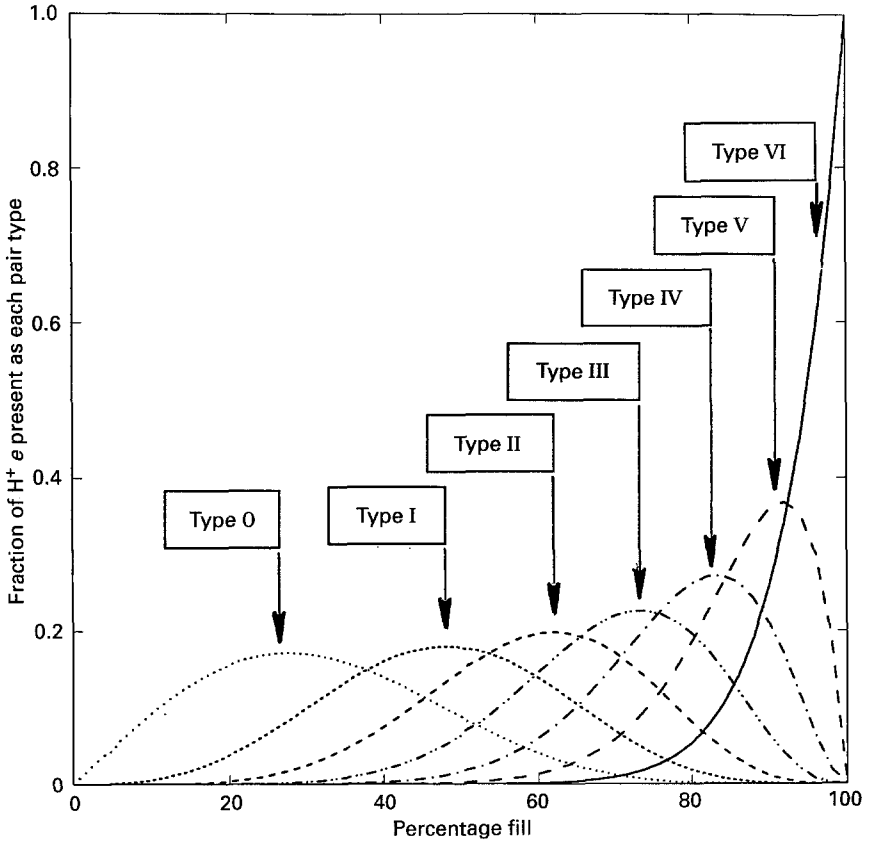

Fig. 8. Pair types against insertion level. Key: (. . . .) type 0; (- - - -) type I; (– – – –) type II; (– · – · – · –) type III; (– · – · – · –) type IV; (— — —) type V; and (———) type VI.

has a range when it is the dominant type. As already mentioned there is independent evidence that at high levels of insertion, stable microdomains of end-product exist and this behaviour may correlate with the increase in the proportion of inserted species present as type VI pairs. The effect of species and sites being thus removed from contributing to positional entropy may be taken into account by modifying Equation 10 (with $\phi = 2$) to

$$\Delta G_{mix} = -2RT[(0.875 - sB)\ln(0.875 - sB) - s(1 - B)\ln s(1 - B) - (0.875 - s)\ln(0.875 - s)] \quad (11)$$

where B is the fraction of inserted H regarded as located and not contributing to positional entropy. Per mole of MnO_nH_s, the number of H^+ and e species each contributing is then $sN_A(1 - B)$ and the number of sites participating is $N_A(0.875 - sB)$. If it is type VI pairs which are located then the value of B can be read directly from Fig. 8. In principle however not only type VI pairs but also type V pairs which have 5 adjacent pairs might be stabilised sufficiently to be located. In this case B would be equated with the sum of the fractions present as type V and VI pairs given by Fig. 8.

Figure 9 shows the effect on the calculated Gibbs free energy of mixing of postulating location of type VI pairs only, types V and VI, or types IV, V and VI and compares the results with the experimentally derived data. The location of type VI pairs only, makes surprisingly little difference to the calculated Gibbs free energy of mixing and the location of further pair types does not improve agreement with the experimental data convincingly as the shape of the curve changes and a slight inflection which is not evident in the experimental data appears in the calculated curves at high insertion levels.

In an alternative approach account is taken of the blocking effect of adjacent pairs. Again a type VI pair is considered as located as movement of either species of the H^+e pair to a neighbouring site is blocked by the presence of pairs on adjacent sites. However, the species of a type V pair have one avenue of escape as only five of the six adjacent sites are blocked by occupying pairs. This effect may be taken into account by assuming that out of every six type V pairs, five are located and one is contributing to positional entropy. Obviously this idea can be extended to other pair types. Thus for every 6 type II pairs, two are located and four are contributing to position entropy. B in Equation 11 is then given by

$$B = \frac{Z}{100}\left(\frac{f_I}{6} + \frac{f_{II}}{3} + \frac{f_{III}}{2} + \frac{2f_{IV}}{3} + \frac{5f_V}{6} + f_{VI}\right) \quad (12)$$

where f_I, f_{II}, f_{III}, f_{IV}, f_V and f_{VI} are, respectively, the fractions of inserted H present as type I, II, III, IV, V or VI pairs as given in Fig. 8. Z is a factor which takes into account the efficiency with which an adjacent pair blocks movement of the H^+ and e species through the adjacent pair. If the blocking is total, Z is 100.

Figure 10 shows the effect of blocking as expressed by Equation 12 on the Gibbs free energy of mixing calculated using Equation 11. Comparison of 100% and 0% blocking efficiency shows that the blocking concept does improve the match with the experimental

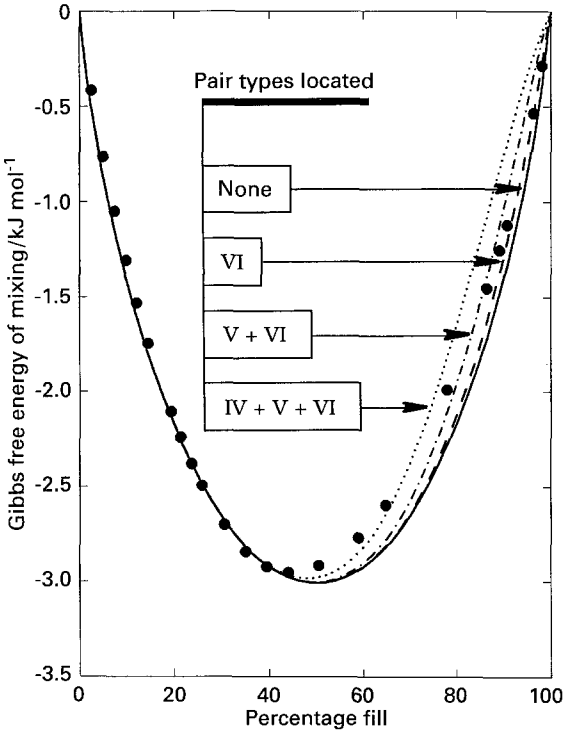

Fig. 9. Effect of pair location on calculated Gibbs free energy of mixing. Key: (•) experimental data derived with Equation 4; (———) no location of pairs; (— — —)Equation 11, type VI located; (- - - - -) Equation 11, types V and VI located; and (. . . . .) Equation 11, types IV, V and VI located.

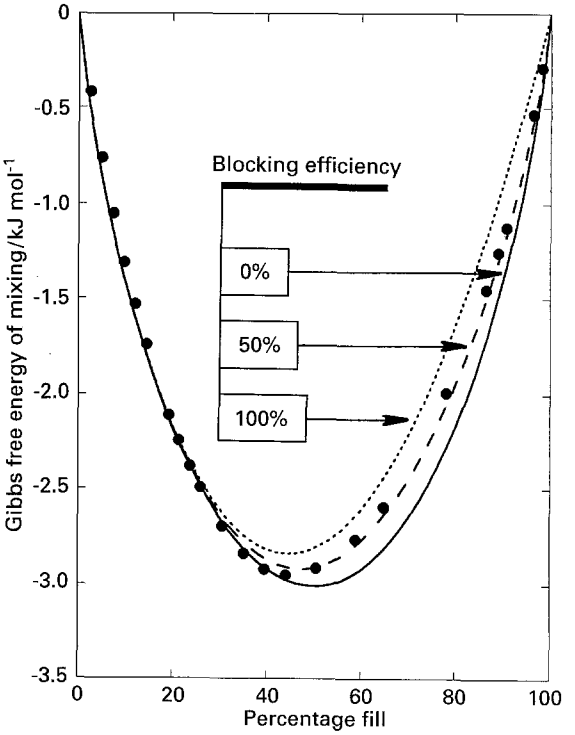

Fig. 10. Effect of blocking by adjacent pairs on calculated Gibbs free energy of mixing. Key: (•) experimental data derived with Equation 4; (———) no blocking; (— — —) 50% efficient blocking; and (- - - - -) 100% efficient blocking.

data. In particular blocking shifts the maximum negative value of the Gibbs free energy of mixing below the position of 50% fill thus bringing the general shape into better conformity with the experimental data. However 100% efficient blocking overcorrects the calculated values and Fig. 10 shows that an assumption of 50% efficient blocking gives a very good match with the experimental data. The assumption of less than total blocking is reasonable as cooperative movement with blocked and blocking species moving at the same time must be a possibility.

4. Conclusions

Comparison between experimental and calculated values of the Gibbs free energy of mixing provides strong evidence that inserted H in solid solutions of MnO_nH_s is present as two thermodynamically independent species H^+ and e at least up to 40% fill.

A planar random insertion model has been developed which shows that at the higher levels of H insertion, microdomains of fully inserted material are present prior to complete insertion.

Good agreement between experimental and calculated values of the Gibbs free energy of mixing at all levels of insertion has been achieved by using the model to take into account the partial blocking of movements of H^+ and e species from an inserted pair by an adjacent pair.

Acknowledgement

One of the authors (SWT) wishes to thank the National Institute for Biological Standards and Control for permission to use their computing facilities for the development of the planar random insertion model.

References

[1] F. L. Tye, 'Electrochemical Power Sources' (edited by M. Barak), Peter Peregrinus, London (1980) p. 50.
[2] F. L. Tye, Proceedings of the 7th Australian Electrochemistry Conference, (edited by T. Tran and M. Skyllas-Kazacos), The Royal Australian Chemical Institute (1988) p. 37.
[3] D. M. Holton, W. C. Maskell and F. L. Tye, 'Power Sources 10', (edited by L. Pearce), The Paul Press, London (1985) p. 247.
[4] K. J. Vetter and N. Jaeger, *Electrochim. Acta* **11** (1966) 401.
[5] S. Atlung, 'Manganese Dioxide Symposium, Vol. 1, Cleveland, 1975', (edited by A. Kozawa and R. J. Brodd), I.C. Sample Office, Cleveland (1975) p. 47.
[6] T. Valand, *Electrochim. Acta* **19** (1974) 639.
[7] F. L. Tye, 'Manganese Dioxide Electrode Theory and Practice for Electrochemical Applications' (edited by B. Schumm, R. L. Middaugh, M. P. Grotheer and J. C. Hunter), The Electrochem. Soc., NJ (1985) p. 301.
[8] W. C. Maskell, J. E. A. Shaw and F. L. Tye, *Electrochim. Acta* **27** (1982) 425.
[9] *Idem, J. Power Sources* **8** (1982) 113.
[10] *Idem, Electrochim. Acta* **28** (1983) 225.
[11] *Idem, ibid.* **28** (1983) 231.
[12] F. L. Tye, *ibid.* **30** (1985) 17.
[13] P. Ruetschi, *J. Electrochem. Soc.* **131** (1984) 2737.
[14] W. C. Maskell, J. E. A. Shaw and F. L. Tye, *Electrochim. Acta* **26** (1981) 1403.
[15] J. P. Gabano, J. F. Laurent and B. Morignat, **9** (1964) 1093.
[16] Y. Uetani, H. Sasama and T. Iwamaru, 'Manganese Dioxide Theory and Practice for Electrochemical Applications' (edited by B. Schumm, R. L. Middaugh, M. P. Grotheer and J. C. Hunter), The Electrochem. Soc., NJ (1985) p. 475.
[17] V. N. Dam'e and E. A. Mendzheritskii, *Elektrokhimiya* **4** (1968) 162.
[18] K. E. Anthony and J. Ostwald, 'Power Sources 10' (edited by L. Pearce), The Paul Press, London (1985) p. 199.
[19] F. L. Tye, *Electrochim. Acta* **21** (1976) 415.
[20] E. A. Guggenheim, 'Thermodynamics', North Holland, Amsterdam (1957) p. 288.
[21] J. Fitzpatrick and F. L. Tye, *J. Appl. Electrochem.* **21** (1991) 130.
[22] G. N. Lewis and M. Randall, 'Thermodynamics' (revised by K. S. Pitzer and L. Brewer), McGraw-Hill, London (1971) p. 280.
[23] D. J. G. Ives, 'Chemical Thermodynamics', Macdonald, London (1971) p. 89.
[24] A. Byström and A. M. Byström, *Acta Cryst.* **3** (1950) 146.
[25] P. M. de Wolff, *ibid.* **12** (1959) 341.
[26] J. H. A. Laudy and P. M. de Wolff, *Appl. Sci. Res.* **10B** (1963) 157.
[27] J. C. Charenton and P. Strobel, *J. Solid State Chem.* **77** (1988) 33.
[28] A. M. Byström, *Acta Chemica Scand.* **3** (1949) 163.
[29] H. Strunz, *Naturwissenshaften* **31** (1943) 89.
[30] P. M. de Wolff, J. W. Visser, R. Giovanoli and R. Brutch, *Chimia* **32** (1978) 257.
[31] R. Giovanoli, 'Manganese Dioxide Symposium, vol. 2, Tokyo, 1980' (edited by B. Schumm, H. M. Joseph and A. Kozawa), I.C. Sample Office, Cleveland (1981) p. 113.
[32] J. Pannetier, Y. Chabre and C. Poinsignon, *ISSI Lett.* **1**(2) (1990) 5.
[33] M. Ripert, C. Poinsignon, Y. Chabre and J. Pannetier, *Phase Trans.* **32** (1991) 205.
[34] W. H. Press, B. P. Flannery, S. A. Tenkolsky and W. T. Vetterling, 'Numerical Recipies in C: the Art of Scientific Computing', Cambridge University Press, Cambridge (1988) p. 212.